

Prediction of switching impulse breakdown voltage of complex gap based on SVM

ZHENPENG TANG¹, YUANCHENG QIN²  , CHANGSHENG WU¹, RONGHUAN MAI¹

¹*Jiangmen Power Supply Bureau Co., Ltd.
China*

²*School of Automation, Wuhan University of Technology
China*

e-mail: qyc@whut.edu.cn

(Received: 08.11.2021, revised: 28.01.2022)

Abstract: Complex gaps may be formed when carrying out live working in substations, while the discharge characteristics of complex gaps are different from those of single gaps. This paper focuses on the prediction of critical 50% positive switching impulse breakdown voltage ($U_{50,crit+}$) of phase-to-phase complex gaps formed in 220 kV substations. Firstly, several electric field features were defined on the shortest discharge path of the complex gap to reflect the electric field distribution. Then support vector machine (SVM) prediction models were established according to the connection between electric field distribution and breakdown voltage. Finally, the $U_{50,crit+}$ data of the complex gap were obtained through twice electric field calculations and predictions. The prediction results show that the minimum $U_{50,crit+}$ of phase-to-phase complex gaps is 1147 kV, and the critical position is 0.9 m away from the high voltage conductor, accounting for 27% of the whole gap. Both critical position and voltage are in good agreement with the values provided in IEC 61472.

Key words: complex gap, electric field features, SVM

1. Introduction

Live working plays an important role in improving power supply reliability [1]. While carrying out live working, floating conducting objects (FCO) may stand between the energized parts and grounded parts. The complex gaps are formed under this circumstance. To ensure the safety of workers [2, 3] and equipment, the minimum approach distances must be determined through the breakdown voltage. A lot of air gap discharge experiments have been carried out to get the discharge characteristics [4–9]. However, it is difficult to take full-scale tests, which is costly and



© 2022. The Author(s). This is an open-access article distributed under the terms of the Creative Commons Attribution-NonCommercial-NoDerivatives License (CC BY-NC-ND 4.0, <https://creativecommons.org/licenses/by-nc-nd/4.0/>), which permits use, distribution, and reproduction in any medium, provided that the Article is properly cited, the use is non-commercial, and no modifications or adaptations are made.

time-consuming. To solve this problem, various empirical and semi-empirical formulas have been proposed by some researchers. In 1984, the calculation formula [9] of the breakdown voltage of the rod-plane under a positive switching impulse was proposed by the CRIEPI laboratory. The formula was accepted by the IEC standard [10]. In 1968, Paris calculated the 50% switching impulse breakdown voltage (U_{50}) of engineering gaps by introducing the gap factor [11]. To some extent, the application of these formulas reduces the dependence on experiments. However, some parameters in these formulas were obtained under specific conditions, and their applicable scope is limited.

A floating conductor will distort the electric field distribution and reduce the dielectric strength of the air gap [12]. In [16], Rizk applied a physical modeling approach to predict the critical 50% switching impulse breakdown voltage ($U_{50,crit}$) of complex gaps containing large floating conductors with different electrode configurations. In [17], the a.c. breakdown voltage of short complex gaps was obtained by a calculation model, the results were in good agreement with experimental data. In [12], a mathematical-physical model which can be applied to obtain the discharge characteristics of phase-to-phase complex gaps of the busbar in substations based on Rizk's empirical formula was established. In [14], there was an obvious difference in discharge characteristics under positive and negative switching impulse voltage.

Some researchers applied artificial intelligence algorithms to predict the breakdown voltage to avoid studying complex discharge processes. In [22], the negative breakdown voltage of the rod-plane, rod-rod and rod-conductor was predicted by the support vector machine (SVM) model. In [18], an SVM model trained by the breakdown voltage data of typical electrodes was used to predict the breakdown voltage of atypical electrodes such as serial gaps, ring gaps and the stranded conductor gap. The power frequency breakdown voltage of rod-plane gaps under rain conditions was predicted in [19]. In [20], the prediction of the breakdown voltage of the complex gap with the helicopter was realized by twice electric field calculations. The prediction of the lightning impulse flashover voltage of insulator string parallel gaps can be realized by extracting features on the shortest discharge path [25]. The genetic algorithm is applied to select 10 from 32 features to predict the breakdown voltage of the sphere gap [26]. These studies provide an idea for predicting the breakdown voltage of complex gaps with small floating conductors. However, the features extracted from discharge channels and shortest discharge paths in these studies are complex. There are various categories of these features. Furthermore, the high-dimensional features make the prediction of breakdown voltage not simple enough. In this paper, the simplified features on the shortest discharge path are proposed, which makes the prediction of breakdown voltage more concise.

A conductive object acquires an intermediate potential and becomes a floating conductor while it is located between two electrodes with different electric potentials. The numbers, dimensions, shapes and geometrical positions of the floating conductor have different effects on the electric strength of air gaps. In any case, especially on the axis of the two conductors, the existence of floating conductors reduces the length of air gaps. The lowest discharge position (critical position) exists in the complex gap, which results in the highest risk level for the live working. Moreover, the positive switching impulse, which is taken into account, is more dangerous than those of negative polarity [24].

When workers use metal tools for live working in substations, a long complex gap with small floating conductors may be formed. There is little research on U_{50} of this kind of complex gap. In this paper, considering the worst case, the SVM algorithm was used to predict the critical 50% positive switching pulse breakdown voltage ($U_{50,crit+}$) and the critical position of complex gaps formed in 220 kV substations.

2. Prediction method of breakdown voltage

The schematic diagram of the phase-to-phase complex gap is shown in Fig. 1. The size and distance of conductors refer to the arrangement of busbars in 220 kV substations [12]. For the convenience of analysis, the metal tool is replaced by a small floating conductor. The small floating conductor divides the phase-to-phase gap into two serial gaps. The gap between the high voltage conductor and the floating conductor is defined as gap 1 (d_1). The gap 2 (d_2) is between the floating conductor and the grounded conductor. d_p is the distance between the high voltage conductor and grounded conductor. Both high voltage and grounded conductors are cylinders with a length of 10 m and a diameter of 0.175 m. The shape of the floating conductor is a rod with a length of 0.3325 m and a radius of 3 cm, both ends of which are hemispherical. This is the worst condition when the center of the high voltage conductor, grounded conductor and floating conductor is at the same height. The whole gap breakdown is related to the breakdown sequence of gap 1 and gap 2. Therefore, the discharge characteristics of complex gaps and single gaps are greatly different.

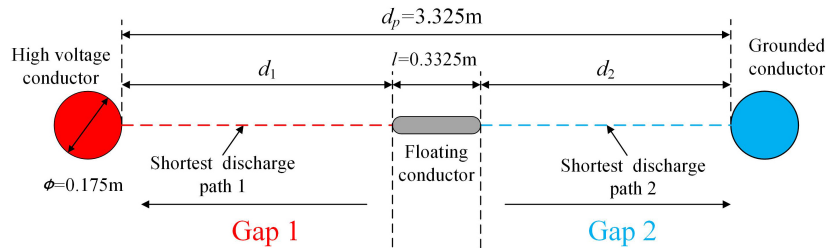


Fig. 1. Schematic diagram of the phase-to-phase complex gap

2.1. Electric field features

The electric field distribution can reflect different electrode shapes and gap distances. It is feasible to predict the breakdown voltage of other gaps without studying the discharge process through SVM models trained by appropriate samples. The key of the proposed approach is to establish the connection between breakdown voltage and electric field distribution. For the complex gap in Fig. 1, some electric field features were extracted from the shortest discharge path of gap 1 and gap 2. In this paper, a feature of the electric field difference integral is defined. In the meanwhile, some parameters are shown in Fig. 2.

There are n sample points in the shortest discharge paths. Parameters S and S_x can be expressed by (1) and (2):

$$S = \int (E - E_{\min}) dl \approx \sum \left(\frac{E_i + E_{i+1}}{2} - E_{\min} \right) (l_{i+1} - l_i) \quad (i = 1, 2, \dots, n-1). \quad (1)$$

$$S_x = \int_{E \geq E_x} (E - E_{\min}) dl \approx \sum_{\frac{E_i + E_{i+1}}{2} \geq E_x} \left(\frac{E_i + E_{i+1}}{2} - E_{\min} \right) (l_{i+1} - l_i) \quad (i = 1, 2, \dots, n-1), \quad (2)$$

where E_{\min} and E_{\max} are the minimum and maximum values of the electric field strength on the shortest discharge paths, respectively. E_x is a predetermined value of the electric field strength.

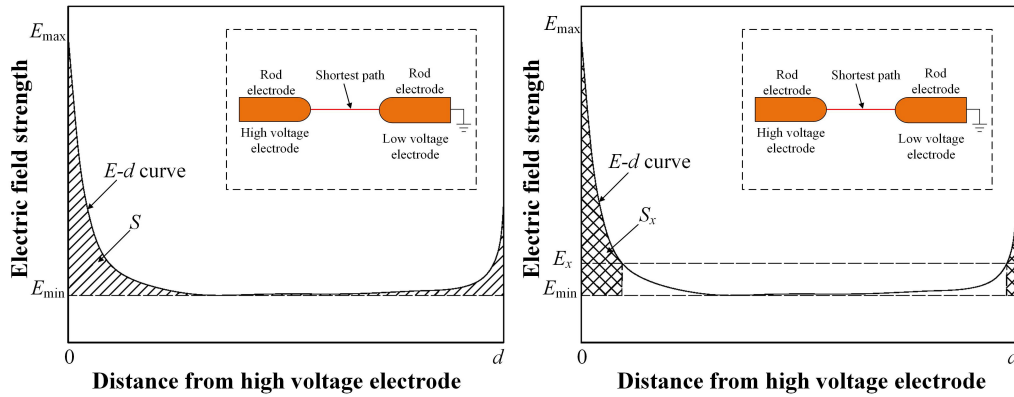


Fig. 2. Schematic diagram of electric field features

E_x increases from 1 kV/cm to 12 kV/cm in a step of 1 kV/cm. The minimum electric field strength on the shortest discharge path is about 1 kV/cm. The average electric field strength is about 6 kV/cm. So, the lower limit of E_x is 1 kV/cm. To enrich the information of electric field features we add that the upper limit of E_x is twice the average electric field strength, that is, 12 kV/cm. Correspondingly, the value of “ x ” in “ E_x ” is also in the range of 1 to 12.

The electric field features $S_{r,x}$ defined in this paper can be calculated from S and S_x as shown in Eq. (3). It can be seen from the calculation method of $S_{r,x}$ that the value range of $S_{r,x}$ is [0, 1]. So, it is unnecessary to normalize the features.

$$S_{r,x} = \frac{S_x}{S}. \quad (3)$$

Meanwhile, the features of electric field integration and path length are also defined. The features of electric field integration and path length are called $V_{r,x}$ and $L_{r,x}$, respectively. $V_{r,x}$ and $L_{r,x}$ are calculated as shown in Eq. (6) and Eq. (9), respectively. The value of E_x is still from 1 kV/cm to 12 kV/cm.

$$V = \int E dl \approx \sum \frac{E_i + E_{i+1}}{2} (l_{i+1} - l_i) \quad (i = 1, 2, \dots, n-1), \quad (4)$$

$$V_x = \int_{E \geq E_x} E dl \approx \sum_{\frac{E_i + E_{i+1}}{2} \geq E_x} \frac{E_i + E_{i+1}}{2} (l_{i+1} - l_i) \quad (i = 1, 2, \dots, n-1), \quad (5)$$

$$V_{r,x} = \frac{V_x}{V}, \quad (6)$$

$$L \approx \sum (l_{i+1} - l_i) \quad (i = 1, 2, \dots, n-1), \quad (7)$$

$$L_x \approx \sum_{\frac{E_i + E_{i+1}}{2} \geq E_x} (l_{i+1} - l_i) \quad (i = 1, 2, \dots, n-1), \quad (8)$$

$$L_{r,x} = \frac{L_x}{L}. \quad (9)$$

2.2. SVM model for breakdown voltage prediction

The SVM is a machine learning algorithm developed on the basis of statistical learning theory. Compared with other artificial intelligence algorithms, the SVM has the following advantages [22]:

1. The computational complexity depends on the number of support vectors rather than the dimension of sample space. It can overcome the dimension disaster caused by mapping from low-dimensional nonlinear space to high-dimensional linear space.
2. The final decision function of the SVM is only determined by a few support vectors. Therefore, the SVM can get much better results than other algorithms on small sample training sets.
3. The learning problem is transformed into convex quadratic programming optimization problems. The SVM can obtain the global optimal solution and solve the local extremum problem of traditional neural networks.

The SVM can be used to solve the binary classification problem. Samples can be divided into two categories by finding a classification line (2D is a straight line, 3D is a plane and multidimensional is a hyperplane). In addition, the classifier is constructed with the function: $\omega^T x_i + b$.

Assume a training sample is $\{(x_1, y_1), (x_2, y_2), \dots, (x_N, y_N)\}$, where $x \in R^n$, $y \in \{-1, 1\}$. The optimal classification hyperplane can be obtained by solving a convex quadratic programming problem [22]:

$$\begin{cases} \min_{\omega, b, \xi} \frac{1}{2} \omega^T \omega + C \sum_{i=1}^N \xi_i \\ \text{s.t. } y_i (\omega^T x_i + b) \geq 1 - \xi_i, \quad \xi_i \geq 0, \quad i = 1, 2, \dots, N \end{cases}, \quad (10)$$

where ω is the vector variable of the hyperplane. C is the penalty coefficient, which determines the classification performance of the SVM. ξ_i is the slack variable. b is the constant to be solved. N is the number of training samples.

The (10) can be solved by solving its dual problem:

$$\begin{cases} \max_{\lambda} -\frac{1}{2} \sum_{i=1}^N \sum_{j=1}^N \lambda_i \lambda_j y_i y_j x_i^T x_j + \sum_{i=1}^N \lambda_i \\ \text{s.t. } 0 \leq \lambda_i \leq C, \quad i = 1, 2, \dots, N \\ \sum_{i=1}^N \lambda_i y_i = 0 \end{cases}, \quad (11)$$

where λ_i, λ_j , represent the Lagrange multiplier.

In practice, it is usually necessary to introduce the kernel function to map original data into high-dimensional feature space in order to solve the problem of linear inseparable. The final decision function after introducing the kernel function can be expressed by (12), according to which the SVM classifies samples.

$$f(x) = \text{sgn} \left(\sum_{i=1}^N \lambda_i y_i K(x_i, x) + b \right). \quad (12)$$

In this paper, the prediction model is established by the LIBSVM toolbox [21]. Furthermore, the linear kernel function is selected as the kernel function used in this paper. There are no parameters to be set for the linear kernel function. So, the optimal hyperplane can be determined only by finding the optimal penalty coefficient C . In this paper, the cross-validation method is used to determine the optimal penalty coefficient C , which makes the classifier have the highest accuracy.

For an air gap with breakdown voltage U_t , the applied voltage [20] is $[0.9U_t, 1.1U_t]$ and the step size is $0.1U_t$. As a result, there are 21 voltages in one gap, which can greatly enrich the training information. $[0.9U_t, 0.99U_t]$ is the withstand interval indicated by -1 and $[U_t, 1.1U_t]$ is the breakdown interval indicated by 1 .

The SVM model can only output -1 or 1 to show whether the air gap breaks down under the applied voltage. Therefore, it is necessary to obtain the specific value of air gap breakdown voltage by the golden section method [22]. The basic principle of the golden section method is to reduce the voltage interval according to the prediction results until the interval length is less than the preset accuracy P . The implementation process is shown in Fig. 3.

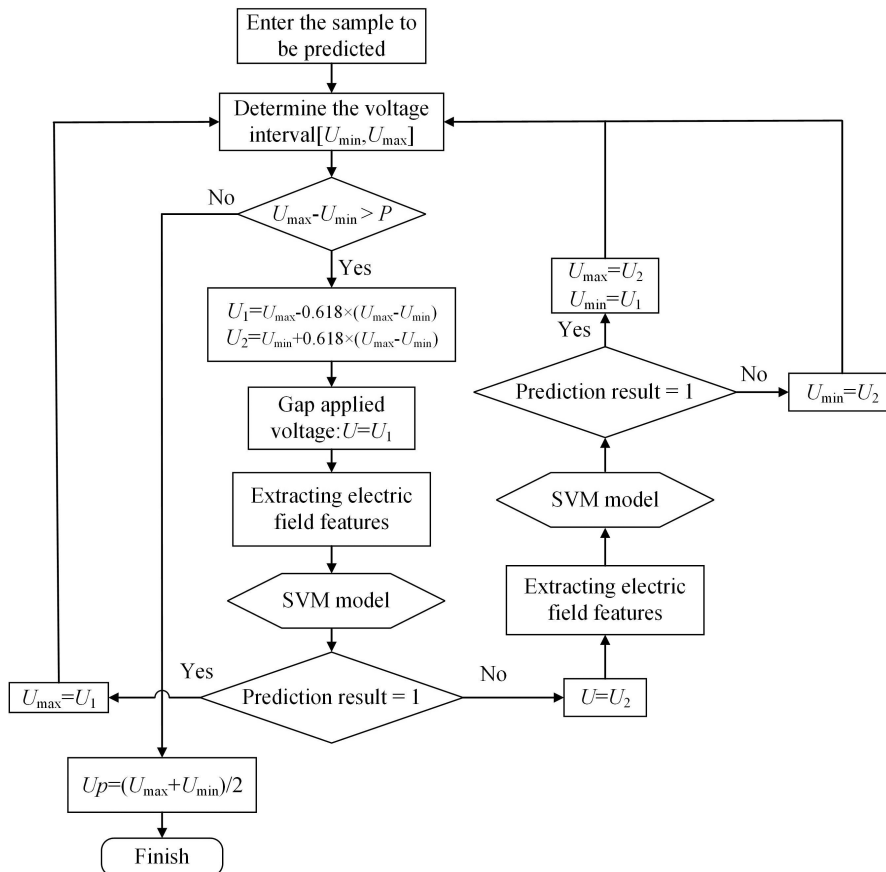


Fig. 3. Schematic diagram of golden section method

2.3. Electric field features selection

In this paper, the Pearson correlation coefficient shown in Eq. (13) is used to measure the correlation between electric field features and breakdown voltage. The absolute value of the coefficient is between 0 and 1. Generally speaking, the absolute value of a coefficient greater than 0.5 indicates that the two variables are significantly correlated. The Pearson correlation coefficients of 12 electric field features in S_{rx} , V_{rx} and L_{rx} were calculated, respectively. The calculation results are shown in Fig. 4.

$$r_j = \frac{\sum_{i=1}^n (X_i - \bar{X})(Y_i - \bar{Y})}{\sqrt{\sum_{i=1}^n (X_i - \bar{X})^2} \sqrt{\sum_{i=1}^n (Y_i - \bar{Y})^2}}, \quad (13)$$

where X_i is the j -th feature of the i -th sample, Y_i is the label of the i -th sample, r_j is the correlation coefficient of the j -th sample, n is the number of samples, \bar{X} is the average value of the j -th feature of all the samples and \bar{Y} is the average value of all the sample labels.

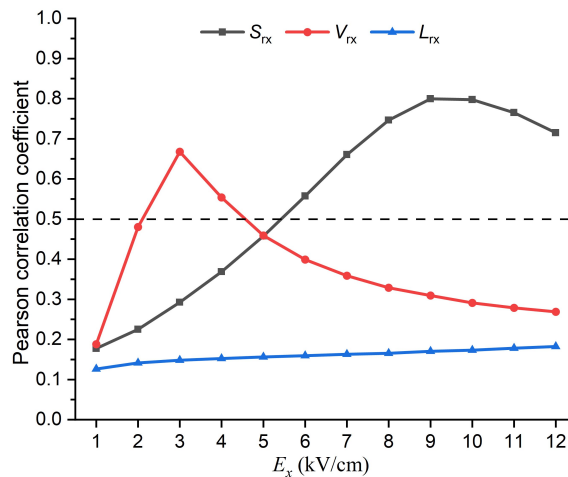


Fig. 4. Calculation result of Pearson correlation coefficient

It can be seen from Fig. 4 that most of the features with the Pearson correlation coefficient greater than 0.5 are in S_{rx} . The results indicate that S_{rx} is significantly related to breakdown voltage. Therefore, S_{rx} is chosen to predict the breakdown voltage.

2.4. Prediction step of complex gap breakdown voltage

A 3D finite element model like Fig. 1 was established by finite element simulation software. The voltage applied to the high voltage conductor was 1 V. The voltage applied to the grounded conductor and truncation boundary was 0 V. The floating conductor was set to floating potential.

In the result of the first electric field calculation, the electric field features were extracted from gap 1 and gap 2, respectively, to predict the breakdown voltage. The breakdown voltage of gap 1 is U_1 and gap 2 is U_2 . It is worth noting that both U_1 and U_2 refer to the voltage applied to the high voltage conductor. The gap with lower breakdown voltage will discharge first, and this gap is called the primary gap. Correspondingly, the other gap is called the secondary gap. U'_1 is the breakdown voltage of gap 1 when gap 1 is regarded as the secondary gap. For U'_2 , the definition is similar.

According to the breakdown sequence of two gaps, the voltage applied to the floating conductor was 1 V or 0 V, and then second electric field calculation was carried out. Only the electric field features of the secondary gap were extracted from the calculation results to predict the breakdown voltage. The larger value of the breakdown voltage of the primary and secondary gaps was taken as the breakdown voltage of the phase-to-phase complex gap. The complete prediction procedure is shown in Fig. 5.

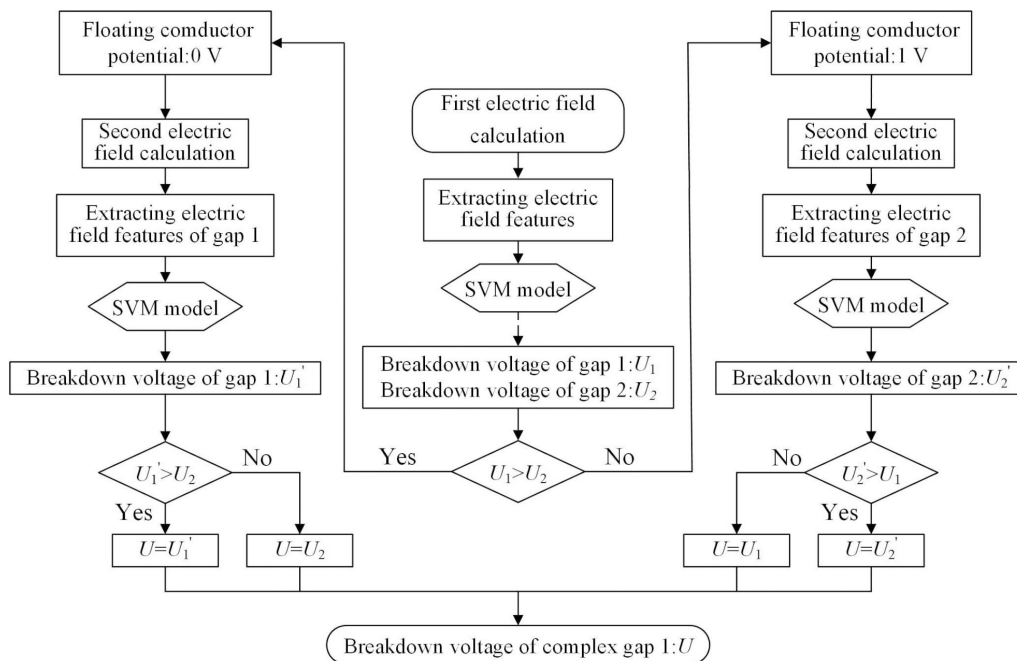


Fig. 5. Prediction process of breakdown voltage in the complex gap

2.5. SVM model

Some researchers [18,20,22] have confirmed that the SVM model trained by the experimental data of typical air gaps can be used to predict the breakdown voltage of other similar gaps. Gap 1 and gap 2 in Fig. 1 are similar to rod-rod air gaps. Therefore, the $U_{50,crit+}$ data of rod-rod gaps were selected as the training sample to establish the SVM model. These $U_{50,crit+}$ data were taken from reference [23] as shown in Table 1.

Table 1. $U_{50,crit+}$ data of rod-rod gaps [23]

Sample no.	d (m)	$U_{50, crit+}$ (kV)	Sample no.	d (m)	$U_{50, crit+}$ (kV)
1	1	561.2	5	3	1263.5
2	1.5	762.4	6	3.5	1411.1
3	2	930.1	7	4	1549.3
4	2.5	1103.2	8	4.5	1684.2

d is the distance between two rod electrodes.

Two of these eight samples were randomly selected as training samples each time. A total of five random selections were made and five SVM models were established with these samples. The training sample numbers and optimal penalty coefficient C of each SVM model are shown in Table 2.

Table 2. Training sample numbers and optimal penalty coefficient C

	Model 1	Model 2	Model 3	Model 4	Model 5
Sample no.	4, 7	1, 5	4, 6	2, 7	4, 8
C	45.2548	106.8913	17805.064	59.7141	16961.7805

These five SVM models were used to predict the $U_{50,crit+}$ data of the samples in Table 1. for verifying the performance of the SVM models. The average of the predicted results of the five SVM models was taken as the $U_{50,crit+}$ data of rod-rod gaps. The comparison between the predicted and the reference value is shown in Fig. 6. The results show that the predicted value

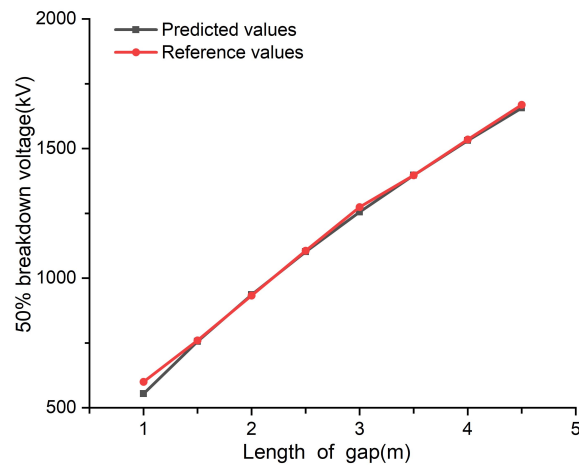


Fig. 6. Comparison between predicted and reference values of $U_{50,crit+}$

is in good agreement with the reference value. The maximum relative error and the average absolute percentage error of the prediction are 7.71% and 1.45%. It is proved that the electric field features proposed in this paper can reflect the connection between electric field distribution and breakdown voltage. These five models were used to predict the $U_{50,crit+}$ data of the complex gap in the next section.

3. Breakdown voltage prediction of complex gap

3.1. First electric field calculation and prediction

In finite element calculation, the size of the mesh has a great influence on the accuracy of the calculation. In this paper, the electric field features were extracted from the shortest discharge paths. Therefore, the area near the shortest discharge paths was refined. Taking the case of $d_1 = 1.4$ m, for example, the electric field distribution of the first electric field calculation is shown in Fig. 7. The electric field distribution of gap 1 and gap 2 is similar to the “U” shape, which is similar to the electric field distribution of rod-rod gaps. It can be seen from Fig. 7 that the electric field is mainly concentrated near the high voltage conductor. It is inferred that gap 1 will discharge before gap 2. In this paper, a total of 29-fold electric field calculations were carried out under different values of d_1 . d_1 increases from 0.1 m to 2.9 m in a step of 0.1 m.

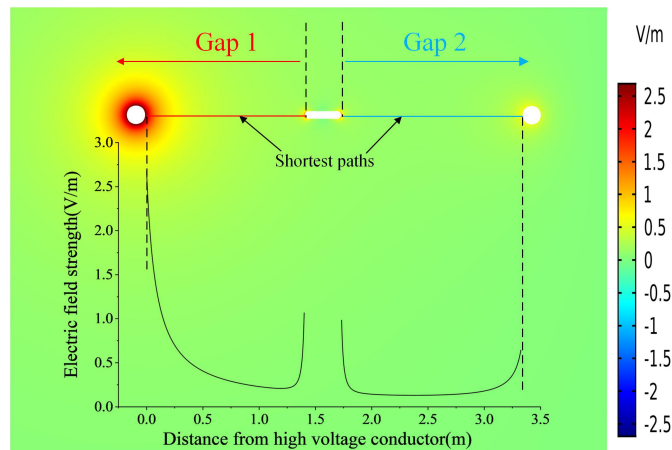


Fig. 7. The electric field distribution of the first electric field calculation

To predict $U_{50,crit+}$, the electric field features of gap 1 and gap 2 were extracted from 29-fold electric field calculations. The prediction results are shown in Fig. 8. It can be seen from Fig. 8 that $U_{50,crit+}$ of gap 1 increases with the enhancement of d_1 . It is obvious that $U_{50,crit+}$ increases with the raising of gap distance. Increasing d_1 limits $U_{50,crit+}$ of gap 2 considerably. When $d_1 = 0.8$ m, $U_{50,crit+}$ reaches its peak. That is because the floating potential on the floating conductor will reduce with the enhancement of d_1 (d_2 is reduced). When d_1 is less than 0.8 m, the drop of floating potential has a greater influence on $U_{50,crit+}$ of gap 2 than the decrease of

gap distance. So, it is necessary to apply a higher voltage to the high voltage conductor to induce enough voltage on the floating conductor to puncture gap 2. When d_1 is less than 2.7 m, gap 1 and gap 2 are regarded as the primary gap and secondary gap, respectively. An opposite result can be obtained while d_1 is greater than 2.7 m.

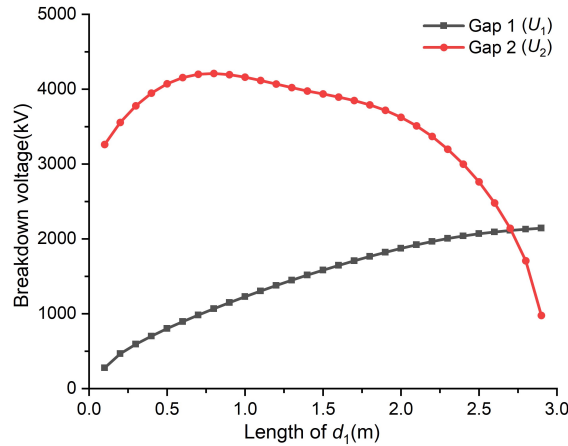


Fig. 8. First breakdown voltage prediction results of gap 1 and gap 2

3.2. Second electric field calculation and prediction

For the second electric field calculation, the arrangement of conductors in the model was the same as that in the first electric field calculation. The voltage of the floating conductor applied was 1 V or 0 V, respectively, while d_1 was less or greater than 2.7 m. Taking the complex gap of $d_1 = 1.4$ m, for example, the electric field distribution during the second electric field calculation is shown in Fig. 9. It can be seen that the result of the second calculation is different from that of

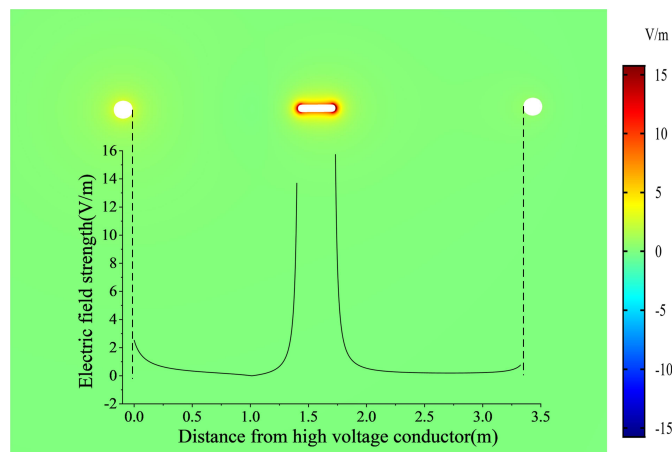


Fig. 9. The electric field distribution of the second electric field calculation

the first calculation. The electric field is mainly concentrated near the floating conductor, and the maximum value of the electric field is much larger than that calculated for the first time.

The prediction results of primary and secondary gaps are shown in Fig. 10(a). It should be noted that the prediction result of the primary gap (black line) is a combination of the smaller values of the two curves in Fig. 8. The larger breakdown voltage of primary and secondary gaps is taken as the breakdown voltage of the complex gap as shown in Fig. 10(b).

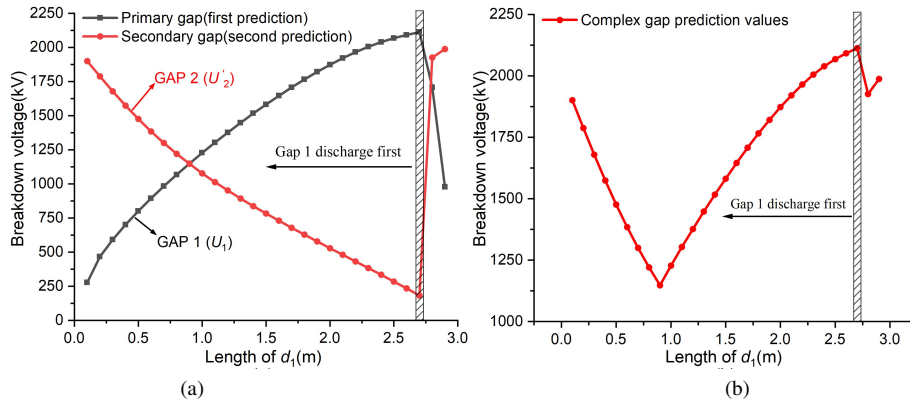


Fig. 10. Prediction results of breakdown voltage in the complex gap

It can be seen from Fig. 10(a) that $U'_2 > U_1$ while d_1 is less than 0.9 m, and $U'_2 < U_1$ while d_1 is greater than 0.9 m. The former one shows that a higher voltage U'_2 is required to puncture gap 2 after gap 1 is first discharged. The latter one shows that the breakdown voltage of gap 1 is enough to puncture gap 2. It can be seen from Fig. 10(b) that when $d_1 < 0.9$ m, $U_{50,crit+}$ decreases as the floating conductor is far away from the high voltage conductor. However, when $d_1 > 0.9$ m, $U_{50,crit+}$ increases with the floating conductor away from the high voltage conductor. The maximum voltage of $U_{50,crit+}$ emerges while the floating conductor stays in the vicinity of the grounded conductor. There is the lowest discharge position at $d_1 = 0.9$ m, which accounts for 27.1% of the length of the gap d_p . The $U_{50,crit+}$ minimum is 1147.38 kV at $d_1 = 0.9$ m. The $U_{50,crit+}$ maximum is 2112 kV at $d_1 = 2.7$ m.

4. Discussion on prediction results

In Annex F of IEC 61472 [24], there is an introduction about the electric strength of complex gaps with a floating conductor in the arrangement of phase-to-phase. This paper is applicable to the phase-to-phase arrangement. In the IEC standard, it is defined as follows:

1. L_f is the length of the original air gap, which is equivalent to d_p in Fig. 1. F is the length of the floating conductor on the axis of the air gap, which is equivalent to l in Fig. 1. Parameter β can be expressed by (14):

$$\beta = \frac{F}{L_f} = \frac{l}{d_p} = 0.3325 \div 3.325 = 0.1. \tag{14}$$

2. D is the length of the air in the complex gap, which is equivalent to $d_1 + d_2$ in Fig. 1. k_f is the floating conductor object factor, and $k_f = 0.95$ can be obtained by looking up the table in IEC 61472 according to the values of L_f and β .
3. U_{L_f} (Critical voltage) is the breakdown voltage of the complex gap when the floating conductor is in the critical position. For the phase-to-phase gap, $d_1/L_f = 0.3$ is the critical position of the complex gap. U_D is the breakdown voltage of the rod-rod gap, and the length of the rod-rod gap is D . U_{L_f} can be calculated by (15).

$$U_{L_f} = U_D \times k_f . \quad (15)$$

In this paper, D is equal to 3 m. In Table 1, the value of U_D is 1263.5 kV while the length of the air gap is 3 m. Therefore, can be obtained by Eq. (15). The comparison of the calculated and predicted values is shown in Table 3.

Table 3. Comparison of calculated and predicted values

	Calculated value	Predicted value	Relative error
Critical voltage	1200.33 kV	1147 kV	-4.44%
Critical position (d_1/L_f or d_1/d_p)	30%	27.01%	-2.99%

As can be seen from Table 3, the relative error is less than 5% in critical voltage and critical position. Therefore, the predicted values are in good agreement with the calculated values. It is feasible to predict the breakdown voltage of the complex gap with a small floating conductor by extracting electric field features from the shortest discharge path of two gaps. The advantage of the prediction method is that it is not necessary to study the specific discharge process.

Theoretically speaking, the proposed method is also applicable to predict the breakdown voltage of complex gaps with large floating conductors. It needs to be further verified by experiments.

5. Conclusions

In this paper, some electric field features on the shortest discharge path of the complex gap were proposed. These electric field features are easy to obtain, and there is no need to normalize them. These electric field features can reflect the connection between electric field distribution and breakdown voltage. Using them to predict the breakdown voltage of the rod-rod gap and the complex gap has achieved good results.

SVM models trained by the $U_{50,crit+}$ data of rod-rod air gaps were established. Through two electric field calculations and predictions, $U_{50,crit+}$ of the complex gap was obtained. The prediction results show that there is the lowest discharge position in the complex gap, that is, the critical position. The critical position is 0.9 m away from the high voltage conductor, accounting for 27.01% of the whole gap. $U_{50,crit+}$ at the critical position is 1147 kV. Both critical position and voltage are in good agreement with the values provided in IEC 61472. The work in this paper can provide a reference for determining the lowest discharge position and the minimum breakdown voltage of complex gaps formed in substations.

Acknowledgements

This work was supported by Science and Technology Project of China Southern Power Grid Co. (No. 030700KK52180142).

References

- [1] Yi H., Kai L., Yong P., Ziming S., Tian W., *Research Status and Development Trend of Live Working Key Technology*, High Voltage Engineering, vol. 40, no. 07, pp. 1921–1931 (2014), DOI: [10.13336/j.1003-6520.hve.2014.07.001](https://doi.org/10.13336/j.1003-6520.hve.2014.07.001).
- [2] Bidi M., *Biological risk assessment of high-voltage transmission lines on worker's health of electric society*, Archives of Electrical Engineering, vol. 69, no. 1, pp. 57–68 (2020), DOI: [10.24425/aec.2020.131758](https://doi.org/10.24425/aec.2020.131758).
- [3] Chang-Qiong Y., Mai L., *Safety evaluation for a high signal operator with electric field exposure induced by contact wires*, Archives of Electrical Engineering, vol. 70, no. 2, pp. 431–444 (2021), DOI: [10.24425/aec.2021.136994](https://doi.org/10.24425/aec.2021.136994).
- [4] Group L.R., *Research on long air gap discharges at les Renardičres; Leader and streamer voltage gradient*, Electra, vol. 23, pp. 53–157 (1972).
- [5] Group L.R., *Research on long air gap discharges at les Renardičres—1973 results*, vol. 35, pp. 49–156 (1974).
- [6] Group L.R., *Positive Discharges in Long Air Gaps at Les Renardičres - 1975 Results and Conclusions*, Electra, vol. 53, pp. 31–153 (1977).
- [7] Carrara G., Thione L., *Switching surge strength of large air gaps: A physical approach*, IEEE Transactions on Power Apparatus and Systems, vol. 95, no. 2, pp. 512–524 (1976), DOI: [10.1109/T-PAS.1976.32131](https://doi.org/10.1109/T-PAS.1976.32131).
- [8] Taniguchi S., Okabe S., Asakawa A., Shindo T., *Flashover Characteristics of Long Air Gaps with Negative Switching Impulses*, Dielectrics and Electrical Insulation IEEE Transactions on, vol. 15, no. 2, pp. 399–406 (2008), DOI: [10.1109/TDEI.2008.4483458](https://doi.org/10.1109/TDEI.2008.4483458).
- [9] Kishizima I., Matsumoto K., Watanabe Y., *New Facilities for Phase-to-Phase Switching Impulse Tests and Some Test Results*, IEEE Power Engineering Review, vol. PAS-103, no. 6, pp. 1211–1216 (1984), DOI: [10.1109/TPAS.1984.318451](https://doi.org/10.1109/TPAS.1984.318451).
- [10] *Insulation coordination Part 2: Application guide*, IEC 60071-2 (2018).
- [11] Paris L., *Influence of Air Gap Characteristics on Line-to-Ground Switching Surge Strength*, IEEE Transactions on Power Apparatus and Systems, vol. PAS-86, no. 8, pp. 936–947 (1967), DOI: [10.1109/TPAS.1967.291917](https://doi.org/10.1109/TPAS.1967.291917).
- [12] Huanqing C., Guiwei S., Zhike W., Ji H., Jing F., Yi C., *Influence of Floating Conducting Objects on Switching Impulse Discharge Characteristics of Phase-to-phase Gap Between Tabular Buses*, High Voltage Engineering, vol. 40, no. 12, pp. 3918–3925 (2014), DOI: [10.13336/j.1003-6520.hve.2014.12.037](https://doi.org/10.13336/j.1003-6520.hve.2014.12.037).
- [13] Baek M.K., Chung Y.K., Han Park I.I., *Experiment and Analysis for Effect of Floating Conductor on Electric Discharge Characteristic*, IEEE Transactions on Magnetics, vol. 49, no. 5, pp. 2323–2326 (2013), DOI: [10.1109/TMAG.2013.2240280](https://doi.org/10.1109/TMAG.2013.2240280).
- [14] Zhenbing Z., Xin W., Hengzhi Z., Wei C., Xiquda Z., Min W., Qing L., Tianjun S., Zezhong S., Hailiang L., *Study on Switching Impulse Discharging Characteristics of Rod-Plate-Rod Combination Gap with Potential Suspension Metal Plate*, Insulators and Surge Arresters, no. 293, pp. 29–35 (2020), DOI: [10.16188/j.isa.1003-8337.2020.01.005](https://doi.org/10.16188/j.isa.1003-8337.2020.01.005).

- [15] Shenghui W., Guanghua Y., Weijiang C., Jun Z., Yujian D., Fangcheng L., Yunpeng L., *Experimental Study on Discharge Characteristics of Combined Air Gap with Floating Potential Conductor*, High Voltage Apparatus, vol. 54, no. 4, pp. 0001–0007 (2018), DOI: [10.13296/j.1001-1609.hva.2018.04.001](https://doi.org/10.13296/j.1001-1609.hva.2018.04.001).
- [16] Rizk F.A.M., *Effect of floating conducting objects on critical switching impulse breakdown of air insulation*, IEEE Transactions on Power Delivery, vol. 10, no. 3, pp. 1360–1370 (1995), DOI: [10.1109/61.400917](https://doi.org/10.1109/61.400917).
- [17] Guanghua Y., Shenghui W., Weijiang C., Huaqian W., Fangcheng L., Jun Z., Yujian D., *Study on the Calculation Method of AC Breakdown Voltage of Complex Air Gap*, High Voltage Apparatus, vol. 56, no. 3, pp. 23–29 (2020), DOI: [10.13296/j.1001-1609.hva.2020.03.004](https://doi.org/10.13296/j.1001-1609.hva.2020.03.004).
- [18] Zhibin Q., Jiangjun R., Congpeng H., Wenjie X., Liezheng T., Daochun H., *A method for breakdown voltage prediction of short air gaps with atypical electrodes*, IEEE Transactions on Dielectrics and Electrical Insulation, vol. 23, no. 5, pp. 2685–2694 (2016), DOI: [10.1109/TDEI.2016.7736827](https://doi.org/10.1109/TDEI.2016.7736827).
- [19] Zhibin Q., Jiangjun R., Wenjie X., Congpeng H., *Breakdown voltage prediction of rod-plane gap in rain condition based on support vector machine*, 2016 IEEE International Conference on High Voltage Engineering and Application (ICHVE), Chengdu, China, pp. 1–4 (2016).
- [20] Zhibin Q., Jiangjun R., Chao L., Qi J., Daochun H.D., *Discharge voltage prediction of complex gaps for helicopter live-line work: An approach and its application*, Electric Power Systems Research, vol. 164, pp. 139–148 (2018), DOI: [10.1016/j.epsr.2018.07.034](https://doi.org/10.1016/j.epsr.2018.07.034).
- [21] Chih-Chung C., Chih-Jen L., *LIBSVM: A Library for Support Vector Machines*, ACM Transactions on Intelligent Systems and Technology, vol. 2, no. 3, pp. 1–27 (2011), DOI: [10.1145/1961189.1961199](https://doi.org/10.1145/1961189.1961199).
- [22] Zhibin Q., Jiangjun R., Wenjie X., Congpeng H., *Energy storage features and a predictive model for switching impulse flashover voltages of long air gaps*, IEEE Transactions on Dielectrics and Electrical Insulation, vol. 24, no. 5, pp. 2703–2711 (2017), DOI: [10.1109/TDEI.2017.006397](https://doi.org/10.1109/TDEI.2017.006397).
- [23] Paris L., Cortina R., *Switching and Lightning Impulse Discharge Characteristics of Large Air Gaps and Long Insulator Strings*, IEEE Transactions on Power Apparatus and Systems, vol. PAS-87, no. 4, pp. 947–957 (1968), DOI: [10.1109/TPAS.1968.292069](https://doi.org/10.1109/TPAS.1968.292069).
- [24] *Live working – Minimum approach distances for a.c. systems in the voltage range 72.5 kV to 800 kV – A method of calculation*, IEC 61472 (2013).
- [25] Zhibin Q., Xuezhong W., Jiangjun R., *Application of a SVR model to predict lightning impulse flashover voltages of parallel gaps for insulator strings*, IEEE Transactions on Electrical and Electronic Engineering, vol. 14, no. 10, pp. 1455–1462 (2019), DOI: [10.1002/tee.22963](https://doi.org/10.1002/tee.22963).
- [26] Zhibin Q., Louxing Z., Yan L., Jianben L., Huasheng H., Xiongjian Z., *Electrostatic Field Feature Selection Technique for Breakdown Voltage Prediction of Sphere Gaps Using Support Vector Regression*, IEEE transactions on magnetics, vol. 57, no. 6, pp. 1–4 (2021), DOI: [10.1109/TMAG.2021.3074035](https://doi.org/10.1109/TMAG.2021.3074035).